

## Discovery of jarosite within the Mawrth Vallis region of Mars: Implications for the geologic history of the region

William H. Farrand<sup>a,\*</sup>, Timothy D. Glotch<sup>b</sup>, James W. Rice Jr.<sup>c</sup>, Joel A. Hurowitz<sup>d</sup>, Gregg A. Swayze<sup>e</sup>

<sup>a</sup>Space Science Institute, 4750 Walnut St., #205, Boulder, CO 80301, USA

<sup>b</sup>Stony Brook University, Department of Geosciences, 255 Earth and Space Sciences Building, Stony Brook, NY 11794-2100, USA

<sup>c</sup>Arizona State University, School of Earth and Space Exploration, P.O. Box 871404, Tempe, AZ 85287-6305, USA

<sup>d</sup>Jet Propulsion Laboratory, Mail Stop 183-501, 4800 Oak Grove Drive, Pasadena, CA 91109, USA

<sup>e</sup>U.S. Geological Survey, Box 25046, Denver Federal Center Mail Stop 964, Denver, CO 80225-0046, USA

### ARTICLE INFO

#### Article history:

Received 20 March 2009

Revised 12 June 2009

Accepted 3 July 2009

Available online 17 July 2009

#### Keywords:

Mars

Mars, Surface

Mineralogy

Spectroscopy

### ABSTRACT

Analysis of visible to near infrared reflectance data from the MRO CRISM hyperspectral imager has revealed the presence of an ovoid-shaped landform, approximately 3 by 5 km in size, within the layered terrains surrounding the Mawrth Vallis outflow channel. This feature has spectral absorption features consistent with the presence of the ferric sulfate mineral jarosite, specifically a K-bearing jarosite ( $\text{KFe}_3(\text{SO}_4)_2(\text{OH})_6$ ). Terrestrial jarosite is formed through the oxidation of iron sulfides in acidic environments or from basaltic precursor minerals with the addition of sulfur. Previously identified phyllosilicates in the Mawrth Vallis layered terrains include a basal sequence of layers containing Fe–Mg smectites and an upper set of layers of hydrated silica and aluminous phyllosilicates. In terms of its fine scale morphology revealed by MRO HiRISE imagery, the jarosite-bearing unit has fracture patterns very similar to that observed in Fe–Mg smectite-bearing layers, but unlike that observed in the Al-bearing phyllosilicate unit. The ovoid-shaped landform is situated in an east–west bowl-shaped depression superposed on a north sloping surface. Spectra of the ovoid-shaped jarosite-bearing landform also display an anomalously high 600 nm shoulder, which may be consistent with the presence of goethite and a 1.92  $\mu\text{m}$  absorption which could indicate the presence of ferrihydrite. Goethite, jarosite, and ferrihydrite can be co-precipitated and/or form through transformation of schwertmannite, both processes generally occurring under low pH conditions (pH 2–4). To date, this location appears to be unique in the Mawrth Vallis region and could represent precipitation of jarosite in acidic, sulfur-rich ponded water during the waning stages of drying.

© 2009 Elsevier Inc. All rights reserved.

### 1. Introduction

Exposures of light-toned layered rocks surrounding the Mawrth Vallis outflow channel were noted by Malin and Edgett (2000). Later observations with the Mars Express Observatoire pour la Minéralogie, l'Eau, les Glaces et l'Activité (OMEGA) imaging spectrometer indicated that these rocks contained widespread occurrences of phyllosilicate minerals (Bibring et al., 2005; Poulet et al., 2005; Loizeau et al., 2007). Higher spatial resolution observations with the Mars Reconnaissance Orbiter (MRO) Compact Reconnaissance Imaging Spectrometer for Mars (CRISM) have revealed that there are several varieties of phyllosilicate minerals present at Mawrth Vallis (Bishop et al., 2008). Reflectance spectra of these minerals can be used to determine a “spectral stratigraphy” for the region. A simplified spectral stratigraphy consists of a basal sequence of Fe–Mg smectites with a distinctive 2.29–2.3  $\mu\text{m}$  absorption overlain by a unit displaying an absorption at

2.2  $\mu\text{m}$ . Variations in the shape and width of the 2.2  $\mu\text{m}$  absorption indicate the presence of different phases including hydrated silica, montmorillonite and kaolinite (Bishop et al., 2008). While acknowledging that it also contains hydrated silica, we henceforth refer to the latter unit as the “Al phyllosilicate” unit. At a number of locations, but not everywhere in the region, there is between the lower Fe–Mg smectites unit and the overlying Al phyllosilicate unit spectral evidence of a phase with a positive spectral slope in the near infrared (NIR) with a change in slope to a flat spectral response at approximately 2  $\mu\text{m}$ . Bishop et al. (2008) interpreted this phase as a ferrous mica but allowed for the possibility of different interpretations. To reflect the ambiguous interpretation of the identity of this phase, we henceforth refer to it as the “Fe2M” phase. Wray et al. (2008) suggested that the Al phyllosilicate layers were draped over the Mawrth Vallis outflow channel topography. However, they were not able to establish whether the underlying Fe–Mg smectite-bearing unit was draped over the pre-existing topography thus leaving open the possibility that the channel was incised through these layers with the Al phyllosilicate layers being deposited later in time. Thus, there is potentially a profound

\* Corresponding author.

E-mail address: [farrand@spacescience.org](mailto:farrand@spacescience.org) (W.H. Farrand).

unconformity between the Fe–Mg smectite – bearing unit and the overlying Al phyllosilicate layers.

Mawrth Vallis is the oldest recognized outflow channel emptying into Chryse Planitia. It occurs in northwest Arabia Terra at the transition from the highlands to the lowlands (with elevations ranging roughly from –1500 m to –3500 m). The channel carves through Noachian-aged ancient cratered terrain and it is the only large outflow channel that does not originate from chaos terrain although Parker (2000) suggested that source chaos region might have been buried by ejecta from the crater Trouvelot.

Bibring et al. (2006) suggested that ancient terrains that show spectral features indicating the presence of phyllosilicate minerals could have formed under environmental conditions where surface and subsurface waters were more alkaline and that a period of global environmental change generated acidic groundwater conditions leading to the deposition of sulfate minerals observed in Terra Meridiani, Valles Marineris and elsewhere (e.g., Gendrin et al., 2005). Here we examine the discovery of a localized deposit in the northern part of the Mawrth Vallis region, present within a single CRISM scene (Fig. 1), that has spectral features of the ferric sulfate mineral jarosite [(Na, K)Fe<sub>3</sub>(SO<sub>4</sub>)<sub>2</sub>(OH)<sub>6</sub>] that would indicate acidic ground or surface waters in the Mawrth Vallis region.

## 2. Data

Numerous CRISM HRL and FRT scenes have been collected over the Mawrth Vallis region to evaluate its viability as a possible Mars Science Laboratory landing site (Grotzinger, 2009). The CRISM instrument is described more fully in Murchie et al. (2007), but briefly it utilizes two spectrometers, an “S” spectrometer covering the wavelength region from 0.36 to 1.05 μm, and an “L” spectrometer covering the wavelength region from 1.0 to 3.9 μm. Spectral resolution is approximately 6.55 nm/channel and spatial resolution in its “full resolution targeted” or FRT mode is 15–19 m/pixel. In order to avoid effects from thermal emission in the “L” spectrometer data, here we utilize only channels below 2.65 μm. While there is also information to be derived from “S” spectrometer data, atmospheric dust has a greater influence at these shorter wavelengths. Mars also has inherently low reflectance, and thus provides low signal, at short wavelengths (less than ~450 nm). CRISM also has a flaw, discussed in more detail in Murchie et al. (2007) caused by a scattered light mask in the VNIR focal plane assembly that results in low response from approximately 610–710 nm, thus except for spectral parameter images calculated

from the “S” spectrometer (using methods from Pelkey et al., 2007), we restrict our spectral analysis to the “L” spectrometer data.

CRISM “L” spectrometer data were converted to apparent surface reflectance and to surface Lambert albedo using two different approaches in order to compare and contrast the results. Data were converted to apparent surface reflectance using a “volcano scan” approach (Langevin et al., 2005; Mustard et al., 2008) implemented in the IDL-based CRISM Analysis Tool (CAT) (Murchie et al., 2007). The data have also been converted to surface Lambert albedo using look-up table values calculated from forward modeling of the scene parameters using the DISORT (Stamnes et al., 1988) radiative transfer model. A description of this approach for the derivation of surface Lambert albedo from CRISM multispectral mapping data was provided by McGuire et al. (2008). Results were generally comparable from the two approaches although the DISORT correction can retain residual atmospheric features, particularly the 2 μm CO<sub>2</sub> feature. Except where noted, the volcano scan corrected data were used here. For later stages of this work we were also able to utilize the denoising approaches in a later release of CAT (Parente, 2008). To help mitigate instrumental effects and to diminish residual atmospheric effects, the data over the region of interest were also divided by a set of pixels with essentially spectrally flat responses drawn from columns in the data over the same range of columns that include the region of interest.

Georeferenced forms of the CRISM imagery were derived by application of latitude and longitude information provided in accompanying CRISM “DDR” (derived data record) files and utilization of the commercial ENVI software.

Various processing approaches were applied to the CRISM data including calculation of a set of standard spectral mapping parameters (Pelkey et al., 2007) and also application of a linear spectral mixture model (Adams et al., 1993) in which averages of spectra from regions of interest taken to best exemplify spectral “endmember” materials were used to derive fraction images (wherein data values ideally go from zero to one with pixels filled with the endmember material having data values of one and pixels devoid of the endmember material having data values of zero) for each endmember.

## 3. Results

As part of a broader examination of the Mawrth Vallis region, we have examined numerous CRISM and OMEGA scenes over this area (Table 1), but in this paper focus on a single CRISM scene,

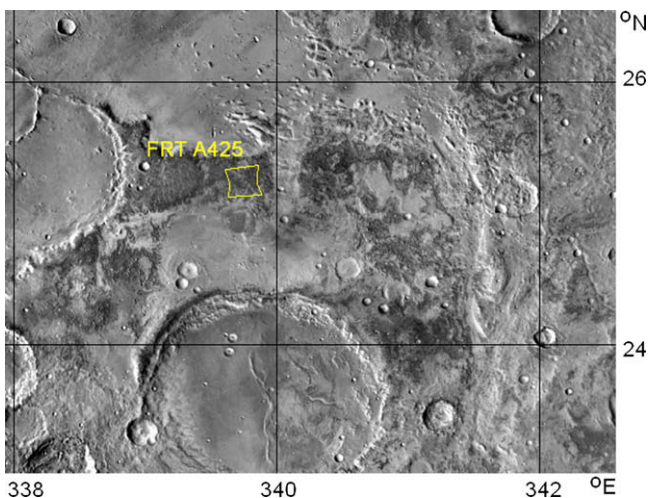


Fig. 1. Mawrth Vallis region shown on a composite of THEMIS day IR images. Location of the CRISM scene referenced in the text is shown.

Table 1

CRISM and OMEGA scenes examined in the conduct of this overall study. Only in the FRT A425 scene have we found spectral evidence of the mineral jarosite.

CRISM scenes	OMEGA scenes
HRL0000285A	Orb0353_3
HRL000043EC	Orb0912_5
HRL00009A5F	Orb0923_5
FRT00003BFB	Orb0934_5
FRT00004ECA	Orb0954_5
FRT0000672C	Orb0967_5
FRT0000863E	Orb0978_5
FRT00008838	Orb0989_5
FRT00009326	Orb1293_0
FRT0000A2C2	Orb1326_1
FRT0000A12A	Orb1337_1
FRT0000A425	
FRT0000A600	
FRT0000A955	
FRT0000AA7D	
FRT0000B3B6	
FRT0000B141	
FRT0000B506	
FRT0000B643	
FRT0000BF57	

FRT0000A425 (henceforward, FRT A425), centered at 25.248°N, 339.745°E (Fig. 1). In the FRT A425 scene, we have identified a location where there is an ovoid-shaped region, approximately 3 km by 5 km in extent, which displays a number of unique spectral characteristics evident even in a three color representation of the scene (Fig. 2A) and especially in a 600 nm “shoulder height” (SH600) parameter image (Fig. 2B), which was derived from the equation in Pelkey et al. (2007):

$$SH600 = R600 / (0.533 * R530 + 0.467 * R680)$$

where R530, R600, and R680 equal the reflectances at 0.53, 0.60, and 0.68  $\mu\text{m}$ , respectively. It can be seen in Fig. 2B that the ovoid-shaped area with the high 600 nm shoulder height is unique within that scene in terms of having high values of that spectral parameter. Fig. 2C shows a composite of fraction images derived from spectral

mixture analysis (SMA) of the scene. In this image, the red channel is assigned to surfaces displaying the 2.2  $\mu\text{m}$  absorption (characteristic of the Al phyllosilicate unit), green to surfaces displaying a 2.29  $\mu\text{m}$  absorption (attributed to nontronite in the Fe–Mg smectite unit) and blue to surfaces displaying a spectral signature with a positive sloping NIR spectrum (the Fe2M spectral signature referenced earlier). In this representation, the ovoid-shaped region shows up in a magenta color. Image endmember spectra used in the SMA (including a spectrally neutral endmember not included in the composite of Fig. 2C) are shown in Fig. 3A (with their extraction locations shown in Fig. 4) and spectra of potentially analogous minerals from the CRISM spectral library and from Cloutis (unpublished data) are shown in Fig. 3B.

An average of pixels selected from within the ovoid-shaped region from CRISM “L” spectrometer data and atmospherically

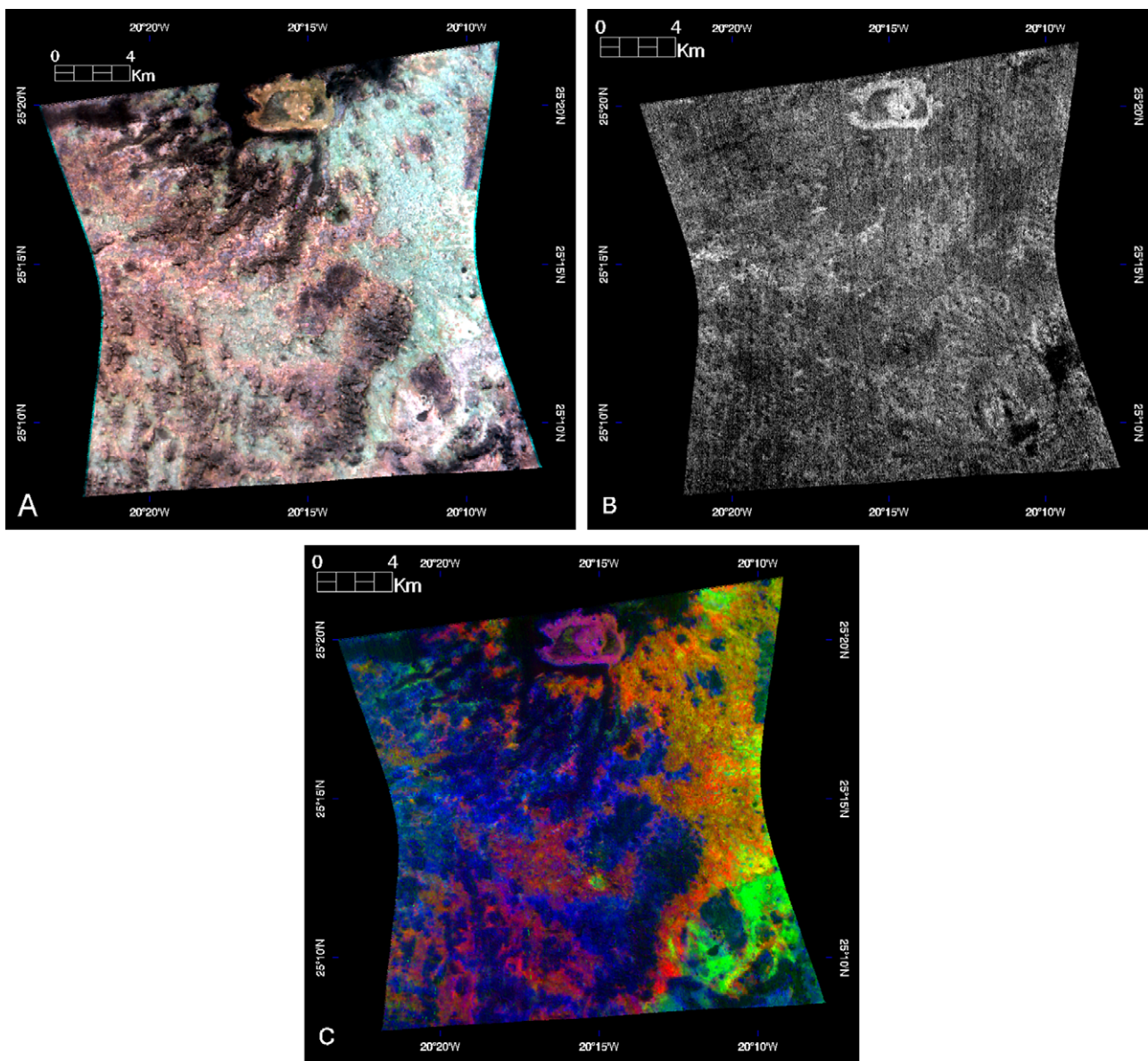


**Fig. 2.** (A) Georeferenced CRISM FRT A425 scene RGB composite of bands centered at 2.5, 1.5 and 1.08  $\mu\text{m}$ . North is at the top of this and other images shown. This band combination enhances differences in surface compositions. Surfaces that display a 2.2  $\mu\text{m}$  absorption appear cyan, those with the nontronite and Fe–Mg smectite compositions are white in this instance and the surfaces with the “Fe2M” spectral signature are more pink. The anomalous ovoid shaped region appears tan to brown in this representation. (B) 600 nm shoulder height image from the CRISM “S” spectrometer. The anomalous ovoid shaped area discussed in the text has higher 600 nm shoulder height values. (C) composite of SMA fraction images (red = Al phyllosilicate unit; green = Fe–Mg smectite unit, blue = Fe2M phase). Anomalous ovoid shaped region appears magenta in this representation. (For interpretation of the references to color in this figure legend, the reader is referred to the web version of this article.)

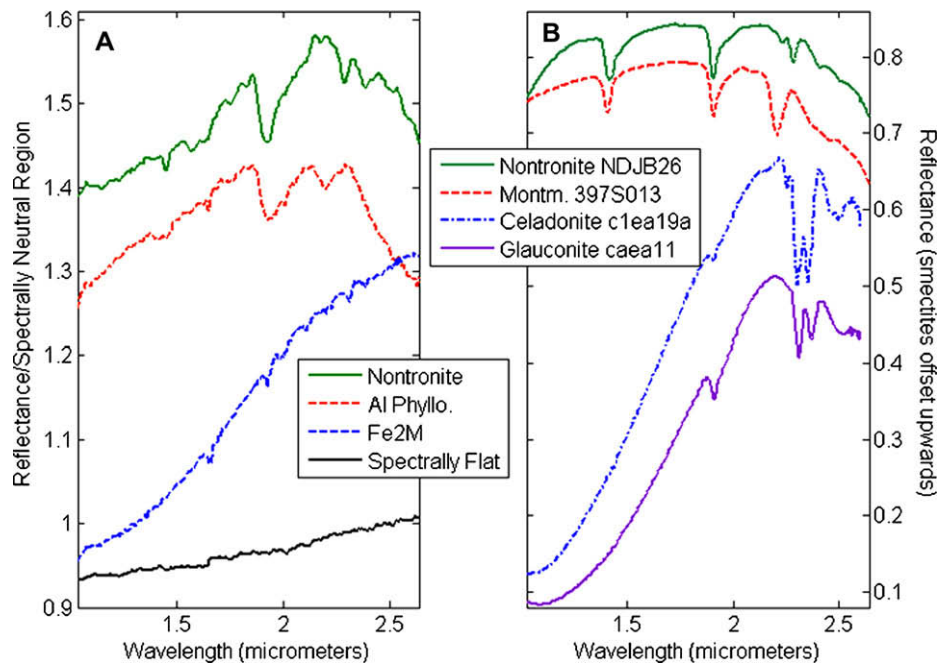


**Fig. 3.** (A) Image endmember spectra from CRISM scene FRT A425 used in the SMA of Fig. 2C. Spectra are from data corrected by the “volcano scan” approach and divided through by a spectrally featureless region. (B) Laboratory spectra of minerals analogous to the image endmembers with absorption features (the featureless “Neutral” endmember is not represented by an analog). The nontronite and montmorillonite spectra are from the CRISM spectral library. Celadonite and glauconite were cited by Bishop et al. (2008) as possible analogs to the “Fe2M” endmember (spectra here from E. Cloutis, unpublished data).

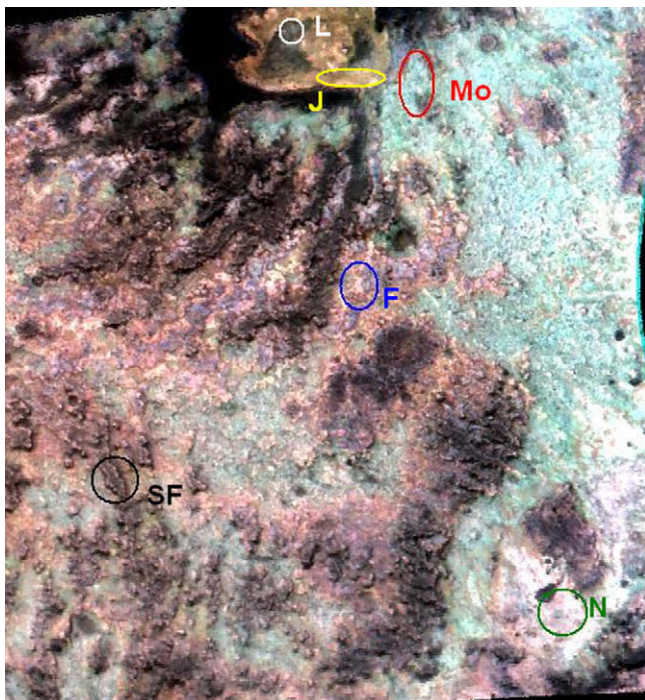


**Fig. 4.** Subsection of Fig. 2A showing areas from which endmember spectra in Fig. 3A and spectrum in Figs. 5 and 12 were drawn from. “N” = nontronite, “Mo” = montmorillonite, “F” = Fe2M, “SF” = spectrally flat, “J” = jarosite, “L” = low region.

corrected by the volcano scan approach is shown in Fig. 5A. In order to mitigate instrumental noise and the incomplete removal of the atmospheric CO<sub>2</sub> absorptions, this spectrum was divided by an average of spectrally flat pixels drawn from columns in the image coinciding with the ovoid-shaped region. The average of the spec-

trally flat pixels is also shown as is the resulting ratio spectrum, which has been scaled to fit on the same plot as the numerator and denominator spectra. Overlaid on the ratio spectrum is that same spectrum that was smoothed using the Savitsky–Golay filter (Gander and von Matt, 1991). Arrows indicate an asymmetric band centered at 2.265 μm and a weaker band centered at 1.915 μm (note that the apparent band at 1.65 μm is an instrumental artifact). Fig. 5B shows the Savitsky–Golay smoothed CRISM spectrum over the region from 2 to 2.65 μm compared with a library spectrum of the ferric sulfate mineral jarosite from the CRISM spectral library ([http://pds-geosciences.wustl.edu/missions/mro/spectral\\_library.htm](http://pds-geosciences.wustl.edu/missions/mro/spectral_library.htm)). There are good matches to the 2.265, 2.46, 2.51, and 2.62 μm absorptions.

The observed absorption band with a minimum at 2.265 μm is asymmetric with a subsidiary band with a minimum at 2.212 μm. Library spectra of jarosite also show this asymmetry and this weaker band with the strength and position of this band being different between Na and K jarosites. Fig. 6 shows, over a spectral subset from 2.135 to 2.245 μm, continuum-removed versions of the CRISM spectrum, and USGS library (Clark et al., 2003) Na and K jarosites. The band center of the feature in the CRISM derived spectral average is at 2.212 μm essentially matching that of the library K jarosite PBII whose band center is at 2.213 μm and shortwards of that of USGS Na-jarosite GDS858 at 2.224 μm.

The cause of the 1.92 μm absorption feature could be the result of the presence of various hydrated phases; however, we favor the interpretation of its being due to ferrihydrite [Fe<sub>10</sub>O<sub>14</sub>(OH)<sub>2</sub>] which has a 1.925 μm absorption band.<sup>1</sup> In non-linear spectral mixture modeling of the light-toned deposits at Mawrth Vallis, Poulet et al. (2008) found fractions of 10–25% ferrihydrite. Thus, the presence of ferrihydrite in this region would be consistent with the results of Poulet et al. (2008).

<sup>1</sup> Despite its formula, ferrihydrite frequently has surface bound water (Michel et al., 2007).

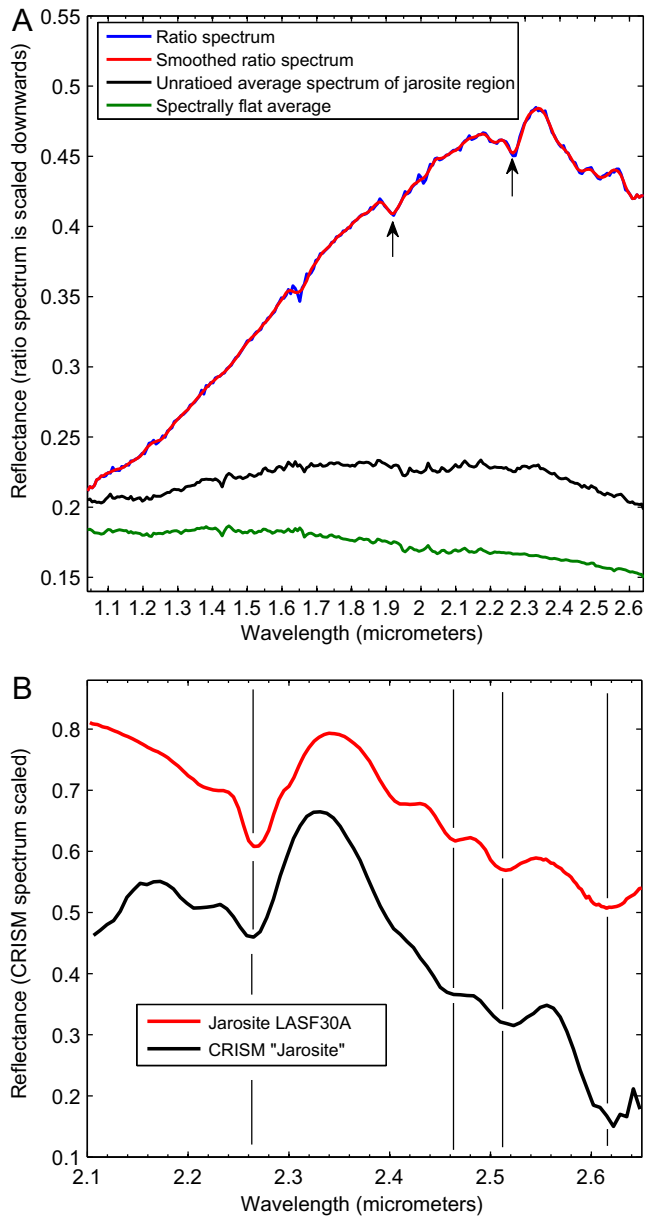


**Fig. 5.** (A) Spectral plots showing, in black, an average of CRISM FRT A425 spectra (from data atmospherically corrected by the volcano scan approach) drawn from spatial elements in the ovoid shaped region that display a 2.265  $\mu\text{m}$  absorption; in green, an average of pixels with a spectrally flat response; in blue, the ratio of the former spectrum to the latter; in red, the ratio spectrum smoothed by a Savitsky-Golay filter. (B) Smoothed CRISM spectrum from Fig. 5A compared with a library jarosite spectrum. Note matches (indicated by discontinuous vertical lines) to bands centered at 2.265, 2.46, 2.51 and 2.62  $\mu\text{m}$ . (For interpretation of the references to color in this figure legend, the reader is referred to the web version of this article.)

Two spectral absorptions typically associated with jarosite, namely absorptions centered at 1.47 and 1.85  $\mu\text{m}$ , are not observed in the putative jarosite spectra derived from CRISM scene FRT A425. Thin ferric oxide coatings have been shown to diminish the band contrast of the vibrational overtone absorptions at wavelengths short of the 2  $\mu\text{m}$  region in jarosite spectra (Swayze et al., 2000). This type of coating could be acting to diminish the strength of both the 1.47 and 1.85  $\mu\text{m}$  absorptions in the putative jarosite occurrence.

The ovoid-shaped region with the jarosite spectral signature displays evidence of layering as indicated in the HiRISE scene over this region (Fig. 7). The locations of this and other HiRISE subs-scenes presented in this paper is indicated in Fig. 8. The subs-scene in Fig. 7

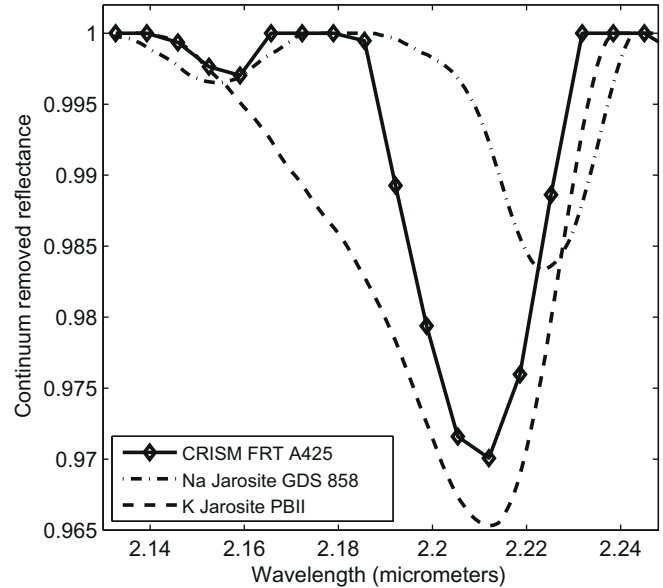


**Fig. 6.** Continuum-removed library spectra in the 2.2  $\mu\text{m}$  region compared with the putative jarosite-bearing spectrum from CRISM scene FRT A425. Note that the best match of the band center of the subsidiary 2.2  $\mu\text{m}$  band from the CRISM spectrum (solid line with diamonds) is to the K jarosite PBII.

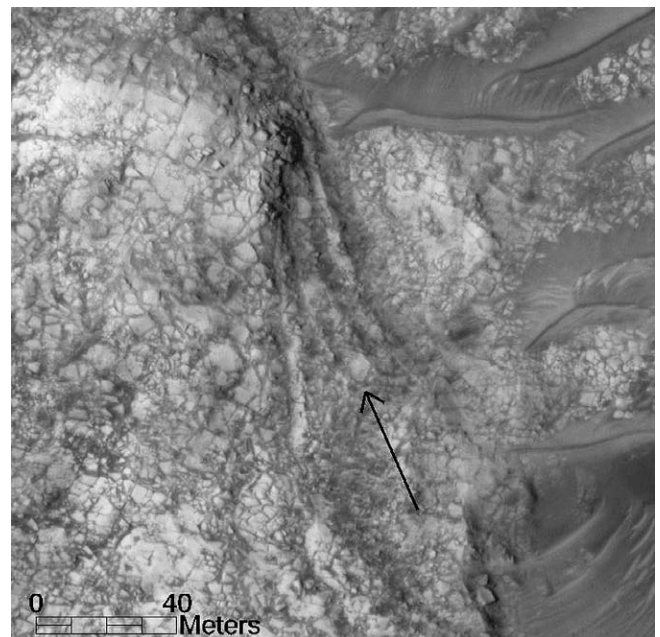


**Fig. 7.** Subs-scene from HiRISE PSP\_007533\_2055 showing layering (indicated by arrow) in the jarosite-bearing unit. North is to the top of the image.

also illustrates the irregular fracture pattern that is representative of this unit. We note that this fracture pattern is essentially the same as that observed elsewhere in Mawrth Vallis for many Fe-Mg smectite-bearing surfaces (Bishop et al., 2008; Wray et al., 2008) as well as within the FRT A425 scene (Fig. 9).

The topographic context of the jarosite-bearing unit is illustrated in Fig. 10. Fig. 10 is an enlarged portion of the three band composite of the CRISM FRT A425 scene from Fig. 2A draped over a digital elevation model (DEM) derived from a High Resolution Stereo Camera (HRSC) scene georeferenced to the CRISM data. The spatial resolution of the CRISM data is nominally 18 m/pixel and that of the HRSC scene (h1564\_0008) is 150 m/pixel. Even in

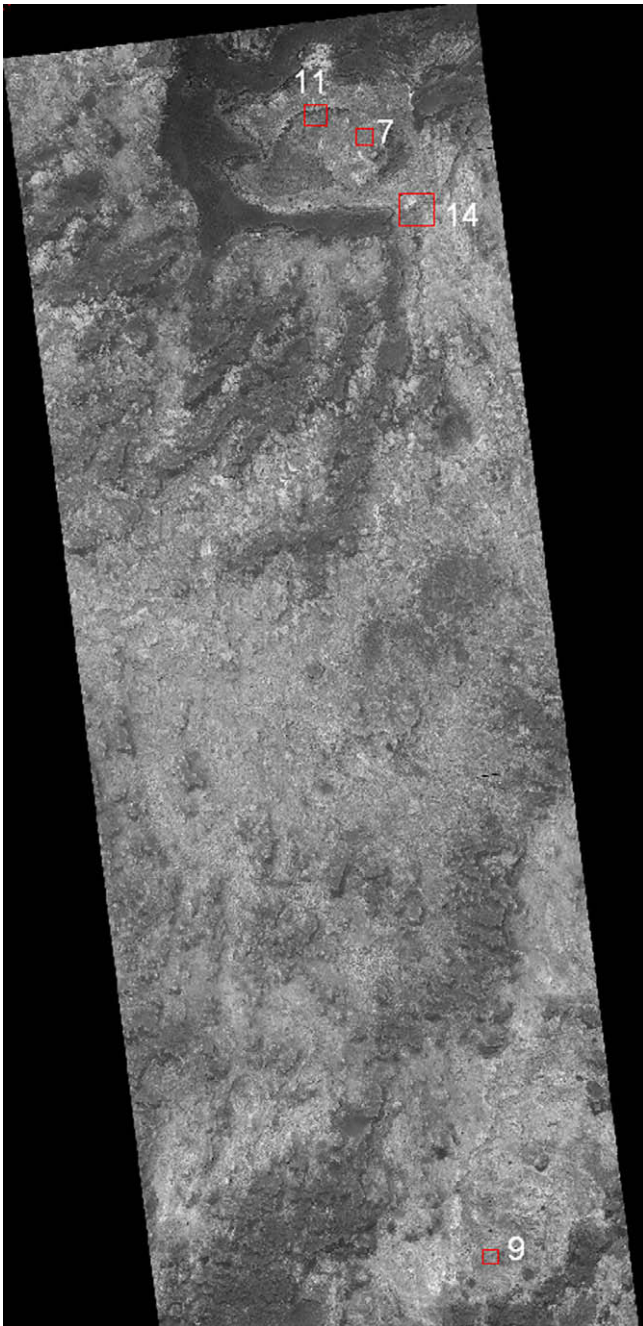


**Fig. 8.** The HiRISE PSP\_007533\_2055 scene with locations of subscenes used here shown.

this three color composite, there is a clear difference between the Al phyllosilicate materials which display a cyan color and the jarosite-bearing surfaces which have an orange-brown color. In this representation, we note that the jarosite-bearing ovoid region lies within a depression. We also point out three areas in Fig. 10, the lowest region, marked by “1”, the jarosite-bearing surfaces marked by “2”, and the Al phyllosilicates marked by “3”. The topographically low region (“1”) has a different color from the jarosite-bearing unit in this three band composite, does not have the elevated 600 nm shoulder height values (in Fig. 2B) and does not have the magenta color in the composite of SMA fraction images in Fig. 2C. A HiRISE subscene over this region (Fig. 11) shows that the topographically low region (“1”) has a higher fraction of drift material than exists over the jarosite-bearing surfaces, but that

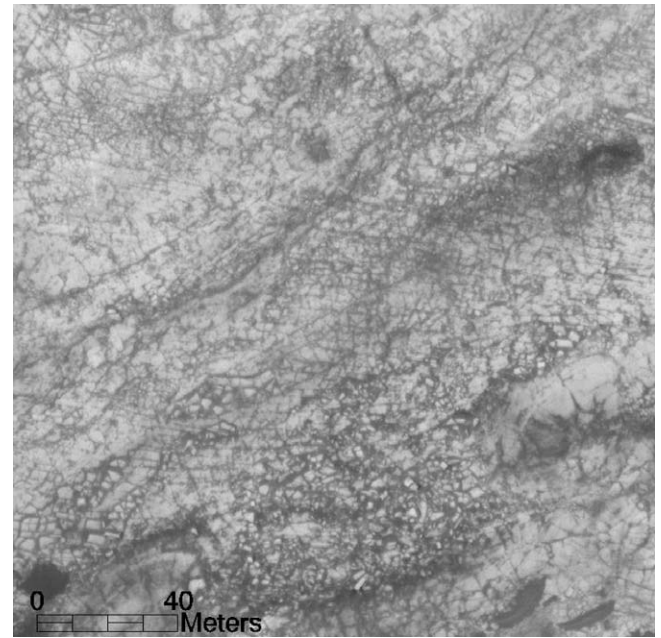


**Fig. 9.** Subscene from HiRISE scene PSP\_007533\_2055 drawn from a region corresponding to the southeast corner of the CRISM FRT A425 scene over a nonjarosite-bearing surface. Note similarity of the fracture pattern of these materials to those in of the jarosite-bearing materials in Figs. 7 and 11.

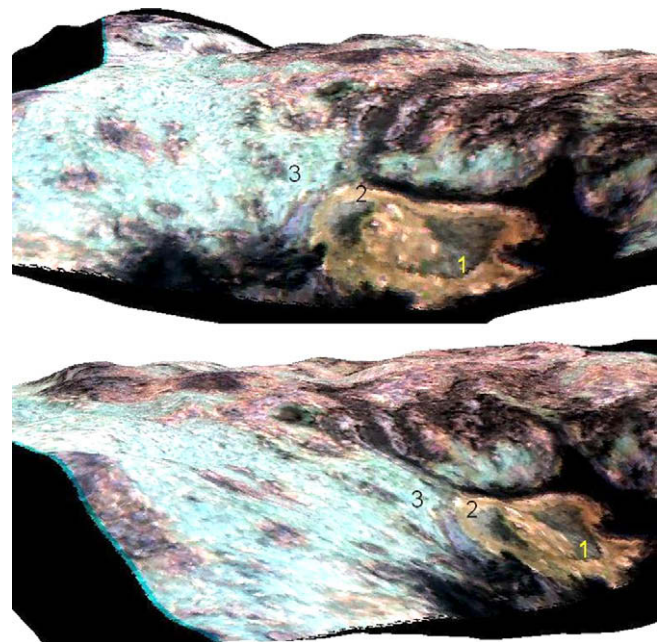


**Fig. 10.** CRISM composite (same band combination as in Fig. 2A) draped over topography derived from HRSC data providing two different perspectives. 1 = lowest portion in ovoid, 2 = jarosite-bearing unit, 3 = Al phyllosilicate unit. Vertical exaggeration is 20×. North is to the bottom of the scene in the top representation and to the lower right in the bottom representation.

there are still exposures of outcrop with fracture patterns similar to those of the jarosite-bearing surfaces. A spectral average of pixels from this low region (drawn from pixels with less drift cover), is shown in Fig. 12. That spectrum is compared to the unsmoothed average spectrum of the jarosite-bearing region from Fig. 5A. In the low “1” region there is still a weak 2.265  $\mu\text{m}$  absorption band, a stronger  $\text{H}_2\text{O}$  absorption with the band center shifted to 1.935  $\mu\text{m}$ , and also a weak 1.45  $\mu\text{m}$  absorption. Thus, there appears

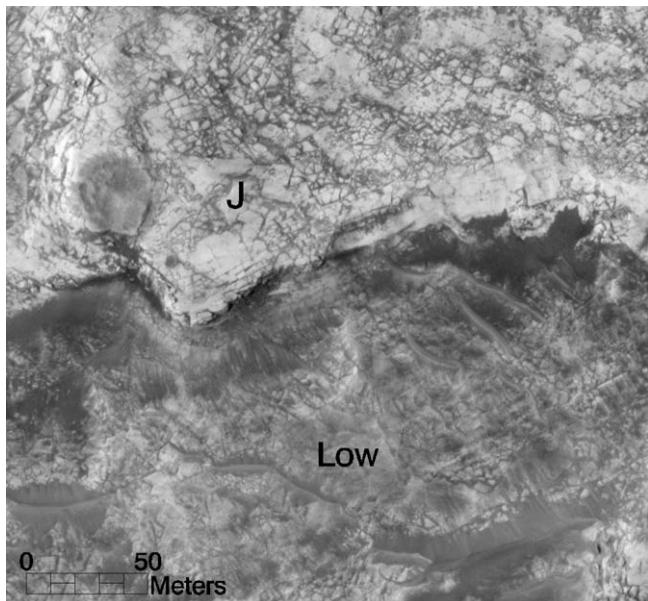


**Fig. 11.** Section of HiRISE scene PSP\_007533\_2055 covering the contact of the jarosite-bearing unit and the lower elevation unit. Lower unit marked with a “Low”. Overlying jarosite-bearing unit marked with a “J”. North is to the top of the image.

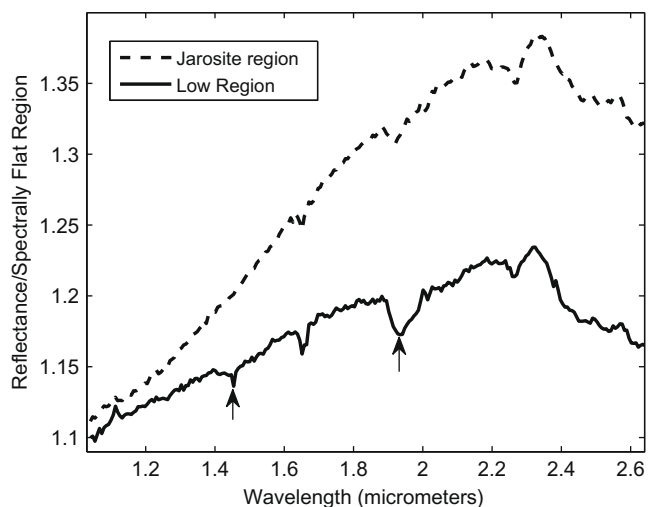


**Fig. 12.** Spectral average of lighter-toned pixels in the topographically low region (marked by “1” on Fig. 10) (solid line) compared to the jarosite-bearing region average from Fig. 5 (dashed line). Arrows indicate the band centers of the low region of hydration features at 1.45 and 1.935  $\mu\text{m}$ .

to be a mixture of materials contributing to the spectrum from exposed surfaces in the low region. Spectra extracted from pixels where drift is the major component do not show these absorption features, so they are interpreted to be from the outcrop. There is thus an indication that jarosite is present as is another hydrated phase or phases. As noted above, ferrihydrite could be present but the 1.935  $\mu\text{m}$  band center is longwards of what is typically seen in ferrihydrite (band center at 1.925  $\mu\text{m}$ ). While we allow for the possibility of other phases potentially accounting for these  $\text{H}_2\text{O}$  absorption bands, in Fig. 13, we show CRISM library spectra of ferrihydrite and schwertmannite  $[\text{Fe}_{16}\text{O}_{16}(\text{OH})_y(\text{SO}_4)_z \cdot n\text{H}_2\text{O}]$ . Ferrihydrite has water absorption bands centered at 1.43 and 1.925  $\mu\text{m}$  and in schwertmannite those band centers are shifted to 1.45 and 1.947  $\mu\text{m}$ . The fact that this band is shifted to a longer wavelength in this lower region could indicate the presence of an

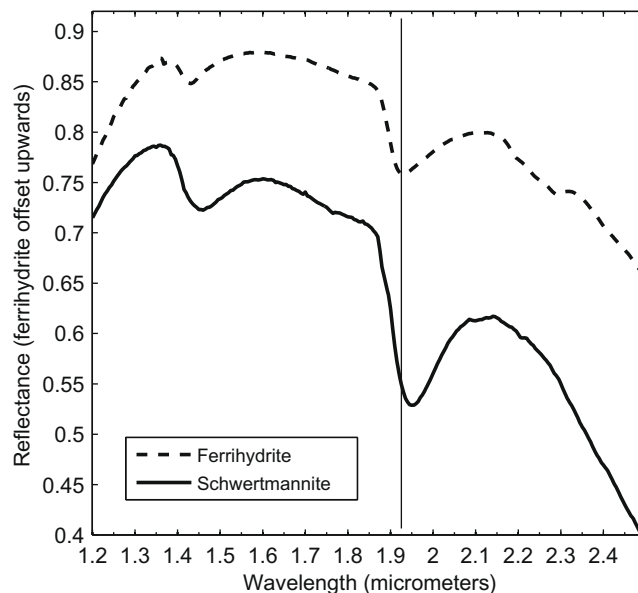


**Fig. 13.** Spectra of ferrihydrite (C1JB130B) and schwertmannite (BKR1JB498A) from the CRISM spectral library. The band center of the ferrihydrite water absorption feature is marked by the vertical line. Schwertmannite has a longer band center for the comparable feature.

additional phase such as schwertmannite although we note that we cannot definitively constrain the identity of the hydrated phases present either in this lower area or in the upper annulus shaped region.

The transition from jarosite-bearing surfaces to the Al phyllosilicate materials is shown in Fig. 14. These surfaces display distinctive fracture patterns (as noted above). Marked by an “F” in Fig. 14 is a relatively unfractured region transitional between the two. A 5 pixel average spectrum from this feature is shown in Fig. 15 showing that this area displays the Fe2M spectral signature.

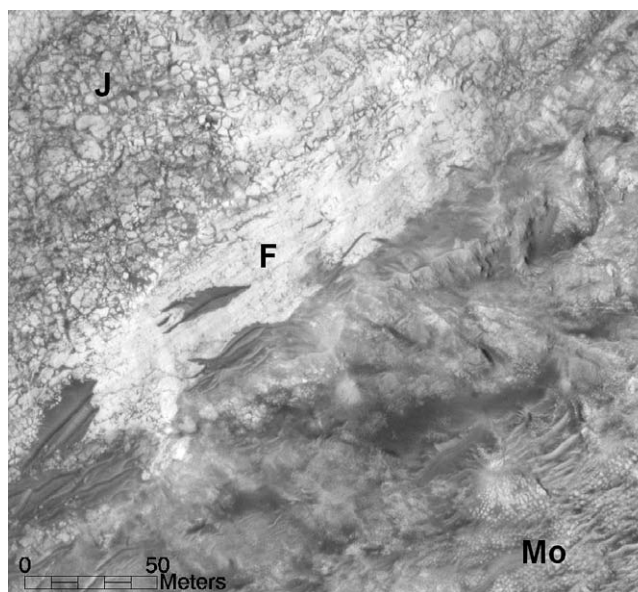


**Fig. 14.** Section of HiRISE scene PSP\_007533\_2055 covering the contact of the jarosite-bearing unit (marked with a “J”) transitioning to the overlying Fe2M materials (marked with a “F”) and the overlying unit with a 2.2  $\mu\text{m}$  absorption, here attributed to montmorillonite (materials marked with “Mo”). The location of this subsense is indicated in Fig. 8 and is also located between the “2” and “3” in Fig. 10.

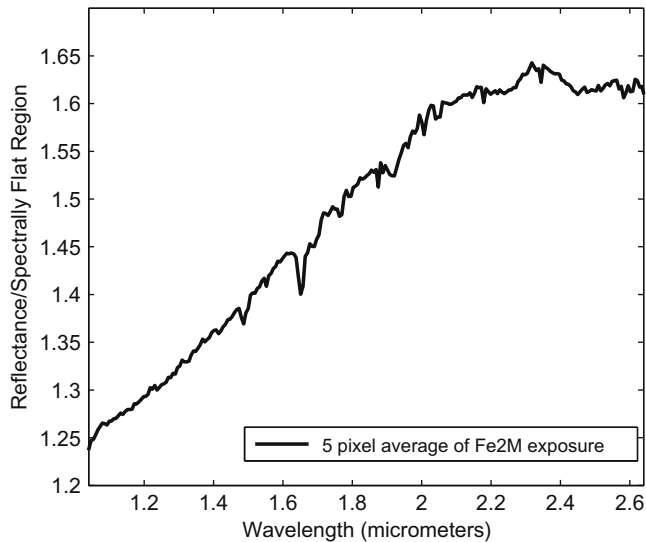


**Fig. 15.** Five pixel average of region marked by “F” in Fig. 14 and which has the characteristics of the Fe2M material described in the text. Spectrum is volcano scan corrected data divided through by spectrally flat region spectrum.

Examination of the fraction image composite in Fig. 2C also shows discontinuous occurrences of blue pixels (indicating higher fractions of the Fe2M spectral endmember) around the border of the jarosite-bearing ovoid. Surfaces displaying this spectral signature were noted by Bishop et al. (2008) as being transitional in the stratigraphy between the Fe–Mg smectite and the Al phyllosilicate layers.

In order to provide a broader view of the topography surrounding the ovoid-shaped region, Fig. 16 shows a THEMIS VIS image covering the jarosite-bearing ovoid-shaped region. As is apparent in the overlay on the HRSC DEM in Fig. 10, the ovoid-shaped region lies within a depression and, in fact, occurs at the lowest point in the approximate east–west transect indicated by the red line in Fig. 16 and shown in the MOLA profile in Fig. 17. In the north–south direction, the location of the ovoid is on a regional gradient descending to the north (although, even at the coarse scale of the

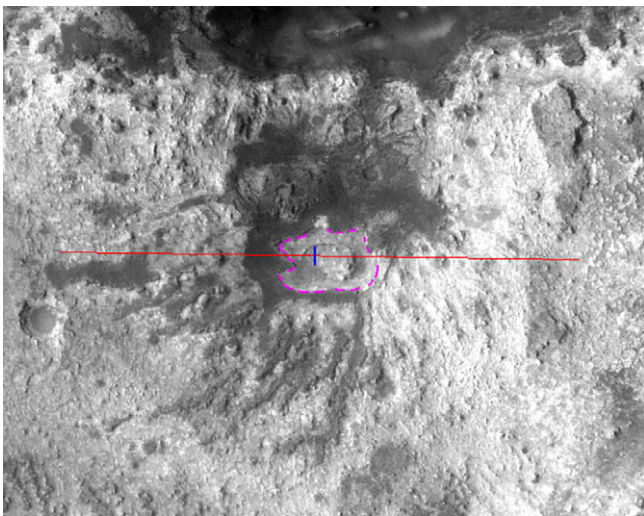


**Fig. 16.** THEMIS VIS image V18760011 with jarosite-bearing ovoid outlined in magenta. Red line indicates MOLA transect shown in Fig. 17. The blue cross-hatch corresponds to the low point in the topographic profile. (For interpretation of the references to color in this figure legend, the reader is referred to the web version of this article.)

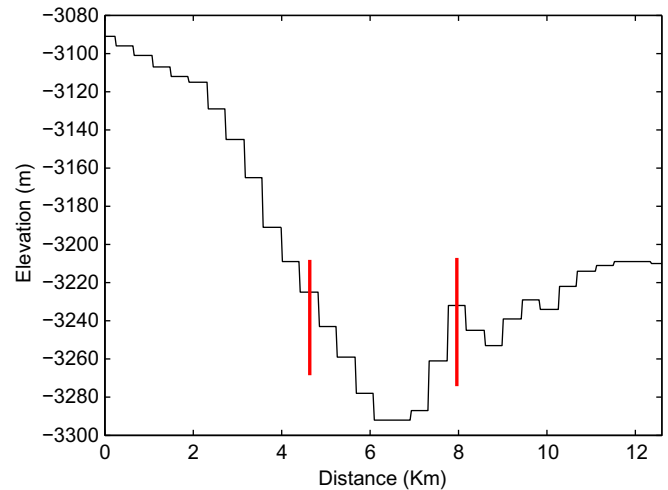


**Fig. 17.** Profile from gridded MOLA topography along the transect shown in Fig. 16. The low point just beyond the 6 km distance point from the start of the transect and corresponds to the blue cross-hatch in Fig. 16 and marks the lowest portion of the ovoid-shaped region. The west and east boundaries of the ovoid are marked by vertical lines.

MOLA gridded topography there does appear to be a bowl shape superimposed on the gradient). It is possible that this depression is the remnant of a highly eroded crater.

This recurrence of jarosite in Mawrth Vallis has not, to our knowledge, been discussed in any other papers examining the area. In this research, in association with a broader examination of the Mawrth Vallis region, we have also examined the OMEGA and CRISM scenes listed in Table 1. We have not observed a jarosite spectral signature in any of these scenes; thus the jarosite occurrence discussed here appears to be an isolated one in this region.

#### 4. Discussion

Several issues related to the jarosite occurrence in Mawrth Vallis bear consideration. The only other (to date) published orbital detection of jarosite on Mars was interpreted by Milliken et al. (2008) as being a hydronium jarosite. The spectral features of the jarosite discussed here appear distinct from that occurrence. Hydronium jarosite has an absorption caused by H<sub>2</sub>O centered at 1.96  $\mu\text{m}$  (Swayze et al., 2008) which is longwards of the observed 1.9  $\mu\text{m}$  region absorptions in this study attributed to adsorbed or bound water. Hydronium jarosite also lacks the subsidiary 2.2  $\mu\text{m}$  absorption feature noted above and highlighted in Fig. 6 as potentially indicating that the jarosite found here is a K jarosite.

There also appears to be a third dimension to the occurrence of the Mawrth Vallis jarosite. That is to say that since the jarosite spectral signature is associated with layered material (Fig. 7) as well as with the topographically low unit (Figs. 11 and 12) that it is not just a coating (as might be produced by acid-fog deposition; Schiffman et al., 2006). To suppose that such an acid-fog coating might be occurring only within this ovoid shaped region begs the question of why it does not occur beyond the confines of this ovoid.

The cause of the relatively high 600 nm shoulder height of the jarosite-bearing materials in the ovoid-shaped region also bears closer examination. Table 2 shows values of 600 nm shoulder height for a set of Mars analog minerals and rocks drawn from the CRISM spectral library. Based on this information, we hypothesize that the high 600 nm shoulder values for the jarosite-bearing surfaces (noted above and shown in Fig. 2B) are likely not related to the presence of the mineral jarosite. As is shown in the dark shaded cells in Table 2, the highest values of this parameter

**Table 2**

VNIR spectral parameter values for Mars analog CRISM library spectra. Note high values of SH600 parameter for goethite and lepidocrocite (dark shaded cells) relative to jarosite (light shaded cells) and other materials.

CRISM library spectra	SH600
Palag tuff 8KR1J8501A	1.0554
Palag tuff 8KR1J8501D	1.0413
Basalt C1FB01	1.0126
Basalt C1FB02	1.0033
Basalt C1FB03	1.0082
Ferrihydrite BKR1JB498A	1.0182
Ferrihydrite BKR1JB499A	1.0322
Goethite BKR1JB047	1.5110
Goethite C1092F54	1.4357
Hematite CAGR04	0.9638
Hematite HMMG01	0.9725
Nontronite CCJB26	1.0730
Nontronite NBJB26	1.0859
Palagonite LAPA03A	1.0994
Palagonite LAPA04A	1.0850
Ferricopiapite BKR1JB620A	1.0118
Jarosite C1092F53	1.1032
K Jarosite BKR1JB406A	1.0358
Schwertmannite BKR1JB130A	1.1989
Schwertmannite C1JB130B	1.1936
Lepidocrocite 892F51	1.2089
Lepidocrocite C1092F56	1.4873

occur for goethite [ $\alpha$ -FeO–OH] and lepidocrocite [ $\gamma$ -FeO–OH], not jarosite. Goethite and lepidocrocite have very similar reflectance spectra and so we refer below primarily to goethite. Identification of goethite in the CRISM data is difficult due to greater effects of dust at shorter wavelengths (where goethite has its diagnostic absorption features) and also to an instrumental flaw in CRISM that covers the spectral range of goethite's 0.66  $\mu$ m absorption (caused by the  ${}^6A_1 \rightarrow {}^4T_2$  transition; Morris et al., 1985). Also, assuming goethite is present, there could be a mixture of goethite, jarosite, and perhaps ferrihydrite and schwertmannite as well. There could also be residual ferrous silicate phases (e.g., pyroxenes; modeled by Poulet et al. (2008) as constituting from 0% to 15% of Mawrth Vallis outcrops). The presence of these other ferric oxyhydroxides and/or ferrous silicates would complicate any identification of goethite by its strong absorption centered near 0.9  $\mu$ m caused by its  ${}^6A_1 \rightarrow {}^4T_1$  transition (Morris et al., 1985). Nonetheless, the anomalous nature of the high 600 nm shoulder heights associated with the jarosite-bearing ovoid suggests the presence of an uncommon phase and crystalline goethite is a good candidate. The goethite, if it is present, could have formed in association with the jarosite or could be the result of the transformation of jarosite. Tosca et al. (2008) noted that oxidation of Fe released from the weathering of basalt under acidic and  $SO_4$ -rich conditions leads first to the formation of schwertmannite, which in turn transforms to jarosite and goethite with the relative percentages of these phases depending on various parameters including, dominantly, pH. These findings also are supported by investigations of terrestrial acid rock drainage environments (e.g., Swayze et al., 2000; Swayze, 2004). For example, Bigham et al. (1992) observed that the end result (in an aqueous environment) of transformation of schwertmannite, jarosite, or at higher pH levels, ferrihydrite is goethite. Therefore, depending on the conditions extant during the formation of the jarosite observed at this location in Mawrth Vallis, the either concomitant or later formation of goethite would be a reasonable outcome. We also note that some of this goethite might be present as the coatings referenced earlier which could be acting to mute the 1.47 and 1.85  $\mu$ m absorptions typically associated with jarosite.

The stratigraphic location of the jarosite-bearing materials identified here is an important issue, but is difficult to determine without some degree of ambiguity. As was noted above, the regional Mawrth

Vallis stratigraphy consists of the Fe–Mg smectites, overlain by Al phyllosilicates with the Fe2M spectral signature materials occurring as a transitional unit between the latter two in many places within the Mawrth Vallis region (Loizeau et al., 2007; Bishop et al., 2008; Michalski and Noe Dobrea, 2007). The Fe–Mg smectite unit is well exposed in the southeastern portion of the FRT A425 scene and fracture patterns of these nontronite-bearing surfaces (Fig. 9) are very similar to those of the jarosite-bearing surfaces shown in Figs. 7, 11 and 14. Also, the position of the Al phyllosilicate layers topographically above the jarosite-bearing unit (Fig. 10) suggests that the Al phyllosilicate layers are stratigraphically above the jarosite-bearing unit; although the possibility of an onlapping stratigraphic transition cannot be excluded given the available data. Alternatively, *in situ* acid sulfate alteration of nontronite and/or other minerals within the upper portion of the Fe–Mg smectite unit might have led to the formation of the observed jarosite. Some commonality between the jarosite-bearing materials and the Fe–Mg smectite materials is suggested by the similarity of the fracture patterns of the two units. Also, as noted in Fig. 14, there appears to be a transition from jarosite-bearing materials to the Fe2M materials to the Al phyllosilicate materials. This appears to favor some alteration of the Fe–Mg smectite materials to jarosite-bearing materials.

Studies of the effect of acid sulfate alteration of phyllosilicate minerals are generally lacking; however, Shaw and Hendry (2009) examined the effect of a low pH solution on smectite, illite, and kaolinite and found that smectite was most susceptible to dissolution and consequent reprecipitation as anhydrite. The latter study was done on a Ca-rich smectite rather than on a Fe or Mg smectite. While it is outside the scope of this study to perform a study on the acid sulfate alteration of nontronite, we posit that it is reasonable to expect that a Fe-bearing sulfate such as jarosite might result from acid sulfate alteration of a Fe-smectite such as nontronite.

The time of formation of the jarosite is also uncertain. If our interpretation of the jarosite as being present in layers that surmount or replace the Fe–Mg smectite layers is correct, there are two primary possibilities for its formation: (1) the jarositic materials were generated before the deposition of the Al phyllosilicate layers or (2) an ancient impact and subsequent erosion exposed the Fe–Mg smectite surfaces in this depression and either jarosite-bearing materials were deposited on top of the Fe–Mg smectite unit (i.e., the jarosite materials would thus have an onlapping relation with the Al phyllosilicates) or the upper portions of the Fe–Mg smectite unit were altered with some jarosite being formed as a result. In the scenario where the observed depression is the eroded remnant of an impact crater, the jarosite could potentially have been formed through hydrothermal alteration with heating derived from the impact as in the model of Newsom (1980). However, the question of why jarosite only formed from the action of this one impact in this one location seems to argue against this possibility.

While the timing of the jarosite formation in the two scenarios noted above is very different, similar formation mechanisms might have acted in either scenario. In order for the jarosite to form, either these beds had some initial complement of sulfide minerals that then altered to form jarosite or there was an influx of sulfur into this location. In the latter scenario, sulfur could have come from volcanic emissions, likely from a volcanic vent beyond the immediate locality (because there are none apparent near Mawrth Vallis). One possibility as to why this location has jarosite, but it has not, to date, been observed elsewhere in the region is that as is apparent in Figs. 10 and 16, the jarosite-bearing ovoid lies at the low point within an east–west depression on the plateau above Chryse Planitia to the northwest. Also, there is a mild bowl-shaped depression superposed on the regional northward-dipping slope. We suggest that in the past this regional gradient might not have been present and that the ovoid might have, in fact, been a local depression where ponded water might have received

sulfur-bearing ash. The consequent evaporation of these waters would have led to the precipitation of the observed jarosite and possible associated goethite, ferrihydrite, and schwertmannite. The fact that jarosite has not, to date, been observed elsewhere in the Mawrth Vallis region seems to suggest that if there was such a lake or ponding of ground water present in association with the current jarosite-bearing ovoid that it was the only such wet feature present at the time of the hypothesized S-bearing ash deposition.

It is interesting to compare the situation that might have existed in this Mawrth Vallis location with that over the larger Meridiani Planum region that has been explored by the Mars Exploration Rover Opportunity (e.g., Squyres et al., 2004a, 2006) and where jarosite has been discovered through *in situ* examination (Squyres et al., 2004b; Klingelhöfer et al., 2004). Hematite present at Meridiani Planum in the form of spherules embedded in, and weathered from, the light-toned Meridiani outcrop and also disseminated in the outcrop has a thermal infrared (TIR) spectral signature most consistent with that of hematite transformed from goethite (Glotch et al., 2004, 2006). While there are other aspects of the respective locations that are clearly distinct (e.g., abundant sulfate minerals at Meridiani, lack of spectral evidence for widespread sulfates at Mawrth Vallis; amorphous silicates at Meridiani, crystalline phyllosilicates at Mawrth Vallis) there might have been some similarities between the locations. Specifically, in both places it appears that there might have been co-precipitation of goethite and jarosite (or transformation of these phases from a schwertmannite precursor), but at Meridiani the goethite transformed to hematite and at this Mawrth Vallis location it did not (hyperspectral TIR data from the Thermal Emission Spectrometer do not show a hematite signature). Thus, there might have been some additional phase of alteration at Meridiani that did not occur at this Mawrth Vallis location resulting in further maturation of Fe-oxides to hematite. At Meridiani, this transformation could have been caused by a more significant time in contact with liquid water, deeper burial resulting in diagenetic heating, or a longer period of exposure to the desiccating martian atmosphere. All of these possibilities, among others, could promote the maturation of Fe-oxide or oxyhydroxide precursors (such as goethite) to hematite.

We also note that the formation of the Mawrth Vallis jarosite and its persistence from early in martian history to today could be the result of only a limited supply of water being present. Elwood-Madden et al. (2004) found that for jarosite to persist after formation from basaltic precursor materials the alteration could not proceed to completion and that the water would need to be removed from the system. We consider a plausible scenario to be one in which an ephemeral lake or ponding of ground water formed in the depression corresponding to the ovoid-shaped region and that it received S-rich ash from a volcanic eruption leading to the creation of acidic waters and the consequent partial transformation of existing materials to jarosite and goethite before arid martian conditions led to the loss of the water.

## Acknowledgments

We thank Kim Lichtenberg of Washington University for doing the conversion to surface Lambert albedo for the CRISM data. Thanks to Ed Cloutis for providing some laboratory spectra through the University of Winnipeg Planetary Spectrophotometer Facility (PSF). This work was funded by NASA's Mars Data Analysis Program.

## References

- Adams, J.B., Smith, M.O., Gillespie, A.R., 1993. Imaging spectroscopy: Interpretation based on spectral mixture analysis. In: Pieters, C.M., Englert, P.A.J. (Eds.), *Remote Geochemical Analysis: Elemental and Mineralogical Composition*. Cambridge University Press, New York, pp. 145–166.
- Bibring, J.P., and 10 colleagues, and OMEGA Team, 2005. Mars surface diversity as revealed by the OMEGA/Mars Express observations. *Science* 307, 1576–1581.
- Bibring, J.P., Langevin, Y., Mustard, J.F., Poulet, F., Arvidson, R., Gondet, B., Mangold, N., Pinet, P., Forget, F., and OMEGA Team, 2006. Global mineralogical and aqueous Mars history derived from OMEGA/Mars Express data. *Science* 312, 400–404.
- Bigham, J.M., Schwertmann, U., Carlson, L., 1992. Mineralogy of precipitates formed by the biogeochemical oxidation of Fe(II) in mine drainage. In: Skinner, H.C.W., Fitzpatrick, R.W. (Eds.), *Biomining Processes of Iron and Manganese, Modern and Ancient Environments*, Catena Supplement 21, pp. 219–232.
- Bishop, J.L., and 11 colleagues, 2008. Phyllosilicate diversity and past aqueous activity revealed at Mawrth Vallis, Mars. *Science* 321, 830–833.
- Clark, R.N., Swayze, G.A., Wise, R., Livo, K.E., Hoefen, T.M., Kokaly, R.F., Sutley, S.J., 2003. USGS Digital Spectral Library splib05a, USGS Open File Report 03-395.
- Elwood-Madden, M.E., Bodnar, R.J., Rimstidt, J.D., 2004. Jarosite as an indicator of water-limited chemical weathering on Mars. *Nature* 431, 821–823.
- Gander, W., von Matt, U., 1991. Smoothing filters. In: Gander, W., Hrebicek, J. (Eds.), *Solving Problems in Scientific Computing Using Maple and MATLAB*. Springer-Verlag, Berlin, pp. 121–139.
- Gendrin, A., and 10 colleagues, 2005. Sulfates in martian layered terrains: The OMEGA/Mars Express view. *Science* 307, 1587–1591.
- Glotch, T.D., Morris, R.V., Christensen, P.R., Sharp, T.G., 2004. Effect of precursor mineralogy on the thermal infrared emission spectra of hematite: Application to martian hematite mineralization. *J. Geophys. Res.* 109, E07003. doi:10.1029/2003JE002224.
- Glotch, T.D., Bandfield, J.L., Christensen, P.R., Calvin, W.M., McLennan, S.M., Clark, B.C., Rogers, A.D., Squyres, S.W., 2006. Mineralogy of the light-toned outcrop at Meridiani Planum as seen by the Miniature Thermal Emission Spectrometer and implications for its formation. *J. Geophys. Res.* 111, E12S03. doi:10.1029/2005JE002672.
- Grotzinger, J.P., 2009. Beyond water on Mars. *Nat. Geosci.* 2, 231–233. doi:10.1038/ngeo480.
- Klingelhöfer, G., and 18 colleagues, 2004. Jarosite and hematite at Meridiani Planum from Opportunity's Mössbauer spectrometer. *Science* 306, 1740–1745.
- Langevin, Y., Poulet, F., Bibring, J.-P., Schmitt, B., Doute, S., Gondet, B., 2005. Sulfates in the north polar region of Mars detected by OMEGA/Mars Express. *Science* 307, 1584–1586.
- Loizeau, D., and 10 colleagues, 2007. Phyllosilicates in the Mawrth Vallis region of Mars. *J. Geophys. Res.* 112, E08S08. doi:10.1029/2006JE002877.
- Malin, M.C., Edgett, K.S., 2000. Sedimentary rocks of Mars. *Science* 290, 1927–1937.
- McGuire, P.C., and 23 colleagues, 2008. MRO/CRISM retrieval of surface Lambert albedos for multispectral mapping of Mars with DISORT-based radiative transfer modeling: Phase 1 – Using historical climatology for temperatures, aerosol optical depths, and atmospheric pressures. *IEEE Trans. Geosci. Rem. Sens.* 46, 4020–4040.
- Michalski, J.R., Noe Dobrea, E.Z., 2007. Ancient clay-bearing sedimentary rocks in the Mawrth Vallis region, Mars. *Geology* 35, 951–954.
- Michel, F.M., Ehm, L., Antao, S.M., Lee, P.L., Chupas, P.J., Liu, G., Strongin, D.R., Schoonen, M.A.A., Phillips, B.L., Parise, J.B., 2007. The structure of ferrihydrite, a nanocrystalline material. *Science* 316, 1726–1729. doi:10.1126/science.1142525.
- Milliken, R.E., and 11 colleagues, 2008. Opaline silica in young deposits on Mars. *Geology* 36, 847–850.
- Morris, R.V., Lauer, H.V., Lawson, C.A., Gibson, E.K., Nace, G.A., Stewart, C., 1985. Spectral and other physicochemical properties of submicron powders of hematite ( $\alpha$ -Fe<sub>2</sub>O<sub>3</sub>), maghemite ( $\gamma$ -Fe<sub>2</sub>O<sub>3</sub>), magnetite (Fe<sub>3</sub>O<sub>4</sub>), goethite ( $\alpha$ -FeOOH), and lepidocrocite ( $\gamma$ -FeOOH). *Geophys. Res. Lett.* 12, 3126–3144.
- Murchie, S., and 49 colleagues, 2007. Compact Reconnaissance Imaging Spectrometer for Mars (CRISM) on Mars Reconnaissance Orbiter (MRO). *J. Geophys. Res.* 112, E05S03. doi:10.1029/2006JE002682.
- Mustard, J.F., and 35 colleagues, 2008. Hydrated silicate minerals on Mars observed by the Mars Reconnaissance Orbiter CRISM instrument. *Nature* 454, 305–309. doi:10.1038/nature07097.
- Newsom, H.E., 1980. Hydrothermal alteration of impact melt sheets with implications for Mars. *Icarus* 44, 207–216.
- Parente, M., 2008. A new approach to denoising CRISM images. *Lunar Planet Sci. XXXIX*, abstract #2528.
- Parker, T.J., 2000. A brief summary of the geomorphic evidence for an active surface hydrologic cycle in Mars' past. *Mars Pol. Sci.* 2000, 4039.
- Pelkey, S.M., and 11 colleagues, 2007. CRISM multispectral summary products: Parameterizing mineral diversity on Mars from reflectance. *J. Geophys. Res.* 112, E08S14. doi:10.1029/2006JE002831.
- Poulet, F., Mangold, N., Loizeau, D., Bibring, J.-P., Langevin, Y., Michalski, J., Gondet, B., 2008. Abundance of minerals in the phyllosilicate-rich units on Mars. *Astron. Astrophys.* 487, L41–L44. doi:10.1051/0004-6361/200810150.
- Poulet, F., Bibring, J.-P., Mustard, J. F., Gendrin, A., Mangold, N., Langevin, Y., Arvidson, R.E., Gondet, B., Gomez, C., and The Omega Team, 2005. Phyllosilicates on Mars and implications for early martian climate. *Nature* 438 (7068), 623–627. doi:10.1038/nature04274.
- Schiffman, P., Zierenberg, R., Marks, N., Bishop, J.L., Dyar, M.D., 2006. Acid-fog deposition at Kilauea volcano: A possible mechanism for the formation of siliceous-sulfate rock coatings on Mars. *Geology* 34, 921–924.
- Shaw, S.A., Hendry, M.J., 2009. Geochemical and mineralogical impacts of H<sub>2</sub>SO<sub>4</sub> on clays between pH 5.0 and –3.0. *Appl. Geochem.* 24, 333–345.
- Squyres, S.W., and 49 colleagues, 2004a. The Opportunity rover's Athena science investigation at Meridiani Planum, Mars. *Science* 306, 1698–1703.

- Squyres, S.W., and 18 colleagues, 2004b. In situ evidence for an ancient aqueous environment at Meridiani Planum, Mars. *Science* 306, 1709–1714.
- Squyres, S.W., and 17 colleagues, 2006. Two years at Meridiani Planum: Results from the opportunity rover. *Science* 313, 1403–1407.
- Stamnes, K., Tsay, S.-C., Wiscombe, W., Jayaweera, K., 1988. Numerically stable algorithm for discrete ordinate method radiative transfer in multiple scattering and emitting layered media. *Appl. Opt.* 27, 2502–2509.
- Swayze, G.A., 2004. Using reflectance spectroscopy to evaluate minerals of environmental concern. In: King, P.L., Ramsey, M.S., Swayze, G.A. (Eds.), *Infrared Spectroscopy in Geochemistry, Exploration Geochemistry, and Remote Sensing*, Mineralogical Association of Canada Short Course Series, vol. 33, pp. 181–196.
- Swayze, G.A., and 10 colleagues, 2000. Using imaging spectroscopy to map acidic mine waste. *Environ. Sci. Technol.* 34, 47–54.
- Swayze, G.A., Desborough, G.A., Smith, K.S., Lowers, H.A., Hammarstrom, J.M., Diehl, S.F., Leinz, R.W., Driscoll, R.L., 2008. Understanding jarosite – From mine waste to Mars. In: Verplanck, P.L. (Ed.), *Understanding contaminants associated with mineral deposits*, U.S.G.S. Circular 1328, 96 pp.
- Tosca, N.J., McLennan, S.M., Dyar, M.D., Sklute, E.C., Michel, F.M., 2008. Fe oxidation processes at Meridiani Planum and implications for secondary Fe mineralogy on Mars. *J. Geophys. Res.* 113, E05005. doi:10.1029/2007JE003019.
- Wray, J.J., Ehlmann, B.L., Squyres, S.W., Mustard, J.F., Kirk, R.L., 2008. Compositional stratigraphy of clay-bearing layered deposits at Mawrth Vallis, Mars. *Geophys. Res. Lett.* 35, L12202. doi:10.1029/2008GL034385.